Fully quantum state-resolved inelastic scattering between He and NO(X2?).

Klos, J.; Aoiz, F.J.; Verdasco, J.E.; Brouard, M.; Marinakis, S.; Stolte, S.

published in
Journal of Chemical Physics
2007

DOI (link to publisher)
10.1063/1.2756826

document version
Publisher's PDF, also known as Version of record

Interactions of transition metal atoms in high-spin states: Cr_2, Sc–Cr, and Sc–Kr

Łukasz Rajchel[a)]
Department of Chemistry, Oakland University, Rochester, Michigan 48309-4477, USA and Faculty of Chemistry, University of Warsaw, Pasteura 1, 02-093 Warszawa, Poland

Piotr S. Żuchowski[b)]
Faculty of Chemistry, University of Warsaw, Pasteura 1, 02-093 Warszawa, Poland

Jacek Kłos
Department of Chemistry and Biochemistry, University of Maryland, College Park, Maryland 20742-2021, USA

Małgorzata M. Szczęśniak
Department of Chemistry, Oakland University, Rochester, Michigan 48309-4477, USA

Grzegorz Chałasiński
Department of Chemistry, Oakland University, Rochester, Michigan 48309-4477, USA and Faculty of Chemistry, University of Warsaw, Pasteura 1, 02-093 Warszawa, Poland

(Received 30 August 2007; accepted 11 October 2007; published online 26 December 2007)

The high-spin van der Waals states are examined for the following dimers: Cr_2 ($^{13}\Sigma_g^+$), Sc–Cr ($^8\Sigma^+$, $^8\Pi$, $^8\Delta$), and Sc–Kr ($^2\Sigma^+$, $^2\Pi$, $^2\Delta$). These three systems offer a wide range of van der Waals interactions: anomalously strong, intermediate, and typically weak. The single-reference [coupled cluster with single, double, and noniterative triple excitations, RCCSD(T)] method is used in the calculations for all three systems. In addition, a range of configuration-interaction based methods is applied in Cr_2 and Sc–Cr. The three dimers are shown to be bound by the dispersion interaction of varying strength. In a related effort, the dispersion energy and its exchange counterpart are calculated using the newly developed open-shell variant of the symmetry-adapted perturbation theory (SAPT). The restricted open-shell time-dependent Hartree-Fock linear response function is used in the calculations of the dispersion energy in Sc–Cr and Sc–Kr calculations, while the restricted open-shell time-dependent density functional linear response function is used for Cr_2. A hybrid method combining the repulsive restricted open-shell Hartree-Fock (or complete active space self-consistent field) interaction energy with the dispersion and exchange-dispersion terms is tested against the RCCSD(T) results for the three complexes. The Cr_2 ($^{13}\Sigma_g^+$) complex has the well depth of 807.8 cm^{-1} at the equilibrium distance of $6.18a_0$ and the dissociation energy of 776.8 cm^{-1}. The octet-state Sc–Cr is about four times more strongly bound with the order of well depths of $^8\Delta > {}^8\Pi > {}^8\Sigma^+$ and a considerable anisotropy. The enhanced bonding is attributed to the unusually strong dispersion interaction. Sc–Kr ($^2\Sigma^+$, $^2\Pi$, $^2\Delta$) is a typical van der Waals dimer with well depths in the range of 81 cm^{-1} ($^2\Delta$), 84cm^{-1} ($^2\Sigma^+$), and 86 cm^{-1} ($^2\Pi$). The hybrid model based on SAPT leads to results which are in excellent qualitative agreement with RCCSD(T) for all three interactions. © *2007 American Institute of Physics*. [DOI: 10.1063/1.2805390]

I. INTRODUCTION

Interactions involving transition metals (TMs) are interesting for a variety of reasons. Because of the incompletely filled $(n-1)d$ subshell, they are open-shell species which can display a wide diversity of bonding types, from van der Waals, to chemical bonds, to multiple metal-metal bonds.[1,2] While the chemically bound TM dimers have been the subjects of intense investigations (see, e.g., Refs. 3 and 4) the van der Waals states of these species have remained virtually unexplored. These spin-polarized states are of great interest to the cold-matter community. Atoms with partially filled $(n-1)d$ subshell and nonzero orbital angular momentum reveal anisotropic properties. That is, in the interactions with other structureless targets, their electronic states further split into manifolds of adiabatic states. The magnitude of this anisotropy is crucial to the success of the collisional cooling of these atoms in a bath of a buffer gas which is the first step in magnetic trapping experiments.[5] Our recent work has shown that in transition metals this anisotropy is unusually small because of the shielding effect of the outer ns^2 electrons.[6] This suppressed anisotropy offers a chance that atoms with nonzero orbital angular momentum may some day be cooled to achieve quantum degeneracy. The atoms with a half-filled $(n-1)d$ subshell are isotropic in the orbital angular momentum sense, but are "magnetically anisotropic" due to the high magnetic moments which give rise to long-range anisotropic

a)Electronic mail: rajchel@oakland.edu.
b)Electronic mail: pzuch@tiger.chem.uw.edu.pl.

magnetic dipole-dipole interactions.[7] These properties are of intense interest to quantum information processing.

The Zeeman relaxation in cold collisions of Sc and Ti with He buffer gas was investigated by Hancox *et al.*[5] The results indicated that compared to the main-group atoms, the rate of inelastic collisions of these atoms with He is several orders of magnitude smaller.[8] Chromium was buffer-gas cooled and magnetically trapped by Weinstein *et al.*[9] Magnetic trapping selects atoms in low-field seeking states (i.e., states the maximum projection of spin onto the magnetic field axis). Collisions of such atoms may lead to inelastic spin depolarization and trap loss. By contrast, if the atoms are trapped in their high-field seeking states, they can be cooled to quantum degeneracy. This task was recently accomplished for chromium by Griesmaier *et al.*[10] Cr-BEC involves a spin-polarized van der Waals state. Further experiments reported observations of Feshbach resonances,[11] which led to the determination of the C_6 and C_8 coefficients for Cr–Cr pair interactions and to the value of the *s*-wave scattering length for the high-spin $^{13}\Sigma_g^+$ state.

The calculations of intermolecular potentials of transition metal atoms are very challenging for *ab initio* theory because of the multireference character of their wave functions, close proximity of excited states, and many types of correlation. In many instances, the symmetry of ground state is uncertain. Gutsev *et al.*[12,13] studied a number of first-row transition metal dimers by the density functional theory (DFT) based on the unrestricted Kohn-Sham treatment. The aim of these studies was to determine ground states. The Cr_2 interaction potentials for the Σ states with total spin S ranging from 0 to 6 was investigated by Pavlović *et al.*[14] using the complete active space second-order perturbation theory (CASPT2). They combined the short- and intermediate-range *ab initio* CASPT2 potentials with the long-range empirically estimated C_6/R_6 term to generate the potential functions for the elastic cross-section calculations for the $^{13}\Sigma_g^+$ state. They found that the value of the *s*-wave scattering length for this state depends dramatically on the choice of the C_6 coefficient. There is also considerable experimental interest in spin-polarized heterodimers of TM atoms. For example, Cr–Mn was recently confined in a magnetic trap at subkelvin temperature using buffer-gas cooling.[15] The interspecies inelastic rate constant was also measured in this experiment. In order to determine if similar cotrapping is possible for Cr with anisotropic TM atoms, one needs to determine the magnitude of the splitting of adiabatic interaction potentials. Sc–Cr can serve as a convenient model for such a determination in addition to being computationally challenging.

The purpose of the present paper is to calculate adiabatic interaction potentials for the highest-spin states of the Cr–Cr and Sc–Cr interactions by a single-reference coupled-cluster method and a variety of multireference treatments including configuration interaction (MRCI), the averaged quadratic coupled-cluster (AQCC), and the configuration-interaction second-order perturbation theory (CIPT2).[16] In order to determine the appropriate methodology to study these systems, we will also explore the newly developed open-shell variant of the symmetry-adapted perturbation theory (SAPT).[17] The third objective of this work is to understand the properties of Sc–Cr in its van der Waals state. This goal will be accomplished by comparing and contrasting this system with a typical van der Waals complex Sc–Kr.

II. THEORY

A. Electronic properties of Cr_2, Sc–Cr, and Sc–Kr

Ground states of Cr and Sc nominally correspond to the $[Ar]3d^54s^1$ and $[Ar]3d^14s^2$ configurations, respectively, and thus result in ^7S and ^2D ground-state terms. The high-spin states correlating with these asymptotes are for Cr_2 the $^{13}\Sigma_g^+$ state, for Sc–Cr the $^8\Sigma^+$, $^8\Pi$, and $^8\Delta$ states, and for Sc–Kr the $^2\Sigma^+$, $^2\Pi$, and $^2\Delta$ states. All calculations were performed in the C_{2v} (for heteronuclear systems) and D_{2h} (for the chromium dimer) abelian point subgroups of $C_{\infty v}$ and $D_{\infty h}$ groups, respectively.

B. Methods

One of the most accurate methods for the study of high-spin open-shell van der Waals states is an open-shell variant of the coupled-cluster (CC) method, such as the partially spin-adapted restricted coupled cluster method with single, double, and noniterative triple excitations RCCSD(T) (Ref. 18) applied within the framework of the supermolecular method. This approach is limited to the states which can be described in zeroth order by a single configuration. When this is in doubt, the MRCI, or some alternative, should be employed. Unfortunately, the lack of size extensivity in many such approaches makes them difficult to apply within the supermolecular framework. The corrections for size extensivity are only approximate and a correction for basis set superposition error cannot be rigorously applied.[19]

Even if the states are nominally single reference, obtaining meaningful CC interaction potentials is not guaranteed. Transition metal dimers are notorious for intruder-state problems, symmetry-breaking, and CC convergence problems. In such circumstances the open-shell SAPT may provide much needed relief. Such theory was proposed in 1980 by Chałasiński and Szalewicz[20] and implemented within the unrestricted Hartree-Fock formalism with uncoupled Hartree-Fock induction and dispersion energies by Cybulski *et al.*[21] The applications included a number of open-shell complexes including systems with degenerate ground states.[22–24] Later a more advanced treatment of open-shell dispersion energy based on time-dependent HF (TDHF) linear response functions (propagators) was developed[25] (see also Hettema and Wormer[26]) and successfully applied to high-spin open-shell systems such as $^5\Sigma_g^+$ state of He_2 (long range) and to a Π-state complex $O(^3P)$-H_2.[27] Recently, a new and promising treatment for high-spin open-shell has been developed which combines SAPT with restricted open-shell Kohn-Sham description of monomers.[17] This approach, referred to as SAPT(DFT), employs the open-shell TDDFT polarization propagators in the treatment of the induction and dispersion energies within adiabatic local density approximation. It is at present applicable to the interactions of nondegenerate high-spin cases.

In this paper the interaction potentials for the above listed states of Cr_2, Sc–Cr, and Sc–Kr are calculated using

RCCSD(T) with large all-electron basis sets the details of which are described in the respective sections. The role of scalar relativistic Douglas-Kroll-Hess[28,29] effects is explored, as well as the influence of core-valence correlation on the potentials. The following multireference approaches were applied to confirm the RCCSD(T) results. In ($^{13}\Sigma_g^+$) Cr_2 the averaged quadratic coupled cluster[30] (AQCC) and CIPT2 (Ref. 16) were employed. CIPT2 is a relatively new hybrid method in which excitations from the active space are treated by MRCI and the remaining excitations by perturbation theory. It proved quite successful in the study of the formidable $X\ ^1\Sigma_g^+$ state of Cr_2.[16] In ($^8\Sigma^+$, $^8\Pi$, $^8\Delta$) Sc–Cr the internally contracted MRCI (Ref. 31 and 32) was applied. CIPT2 and MRCI employed Davidson's correction to approximate the effect of quadruple excitations, denoted CIPT2+Q and MRCI+Q, respectively. The reference functions for all the multireference calculations were obtained from state-averaged complete active space self consistent field (CASSCF) method which employed the full valence active space (unless stated otherwise).

Another confirmation of the obtained potentials and their interpretation on physical grounds is carried out with the SAPT method. The Sc–Cr and Sc–Kr calculations employ SAPT formulated with respect to restricted HF determinants, whereas those for Cr_2 use SAPT(DFT) formulated with respect to restricted Kohn-Sham (KS) determinants. Of particular importance to the goals of this paper are the dispersion energy and its exchange counterpart. The second-order dispersion energy $E_{\mathrm{disp}}^{(2)}$ for a dimer X–Y is calculated from a modified Polder formula

$$E_{\mathrm{disp}}^{(2)} = -\frac{1}{4\pi} v_{rs}^{pq} v_{r's'}^{p'q'} \int_{-\infty}^{\infty} \Pi_{rr'}^{pp'}(i\omega)\Pi_{ss'}^{qq'}(-i\omega)d\omega, \qquad (1)$$

where $\Pi_{rr'}^{pp'}$ are polarization propagators, v_{rs}^{pq} are two-electron integrals, and ω is a frequency. In the above formula, p, p', r, and r' indices run over the orbitals of mononer X, and the remaining set refers to monomer Y orbitals. Polarization propagators are computed with either TDHF (Refs. 33–35) or time-dependent density functional theory (TDDFT). The second-order exchange-dispersion energies are defined with the uncoupled (UC) dispersion amplitudes (either HF or KS). In the SAPT nomenclature they are the $E_{\mathrm{ex\text{-}disp}}^{(20)}$(HF) and $E_{\mathrm{ex\text{-}disp}}^{(2)}$(UCKS) terms (see Ref. 17), respectively. We will refer to them by one generic name, $E_{\mathrm{ex\text{-}disp}}^{(2)}$. The exchange-dispersion terms were calculated within the S^2 approximation, where S denotes the overlap integral.

In the supermolecular approach the interaction potential V of a X–Y dimer (Y is the S-state atom) in a state Λ is calculated from the formula

$$V_\Lambda^M(R) = E_{\mathrm{X-Y},\Lambda}^M(R) - E_{\mathrm{X},\Lambda}^M(R) - E_{\mathrm{Y},0}^M(R) - \Delta E_{\mathrm{rsc},\Lambda}^M(R), \qquad (2)$$

where M stands for a method and Λ is the projection of total orbital angular momentum on the molecular axis and thus refers to Σ, Π, and Δ states. The last term represents the residual size-consistency correction which vanishes when M is a size-extensive method. This term is used to correct for effects which are not removed by the Davidson's correction in MRCI+Q and CIPT2+Q as well as in the non-size-extensive AQCC method. This term ensures that the interaction potentials V vanish in the limit of large R (assumed to be $R=60a_0$). All the terms in Eq. (2) were calculated in the dimer-centered basis set to apply the counterpoise correction[36] (see also Ref. 37). The SAPT components are included in the hybrid model which describes the interaction potential as the following sum:

$$V_\Lambda(R) = V_\Lambda^{\mathrm{CASSCF}}(R) + E_{\mathrm{disp}}^{(2)}(R;\Lambda) + E_{\mathrm{ex\text{-}disp}}^{(2)}(R;\Lambda), \qquad (3)$$

where $V_\Lambda^{\mathrm{CASSCF}}$ [Eq. (2)] is the supermolecular interaction energy obtained at the CASSCF level of theory and the remaining terms are the Λ-dependent dispersion and exchange-dispersion SAPT components. Depending on the circumstances $V_\Lambda^{\mathrm{CASSCF}}$ may be substituted for $V_\Lambda^{\mathrm{ROHF}}$. This model referred to as CAS+disp represents a generalization of the SCF+disp approximation of Ahlrichs *et al.*[38] CAS+disp is based on an assumption that the CASSCF interaction energy obtained with limited active space includes primarily the nondynamic correlation effects and can be used in metal-metal van der Waals interaction.[39] The inability of CASSCF to account for the dispersion energy results from the fact that valence space calculations optimize monomer components of the supermolecular correlation energy. Dispersion energy is the intermolecular electron correlation effect.

The calculations were performed with the MOLPRO package.[40] The SAPT terms were calculated with codes which became incorporated into SAPT2006.[41]

C. Interaction anisotropy

For the interpretation of the anisotropy of the interaction it is useful to work with the isotropic and anisotropic parts of the interaction potentials.[42,43] For a D-state atom interacting with an S-state one, the interaction potential V_Λ is connected with isotropic (V_0) and anisotropic parts of potential (V_2) according to the formula

$$V_0 = \tfrac{1}{5}(V_\Sigma + 2V_\Pi + 2V_\Delta),$$
$$V_2 = V_\Sigma + V_\Pi - 2V_\Delta, \qquad (4)$$

where V_Σ, V_Π, and V_Δ are interaction potentials. The asymptotic regions of potentials obtained with Eq. (4) are used to find isotropic $C_{6,0}$ and anisotropic $C_{6,2}$ dispersion coefficients by fitting them to a function

$$V_\lambda(R) = -\frac{C_{6,\lambda}}{R^6} - \frac{C_{8,\lambda}}{R^8}. \qquad (5)$$

[The C_8 coefficient in Eq. (5) is used to collect higher-rank terms which otherwise may lead to C_6 dispersion coefficient being overestimated.] These calculations are based on the assumption that the long-range interaction energy is governed by the dispersion interaction.

In order to calculate the dispersion coefficients for the Cr_2 system, we have used the following multipole expansion of two-electron integrals appearing in the Casimir-Polder formula:

TABLE I. Comparison of interaction energies of Cr_2 at different levels of theory (all energies in cm^{-1}).

				E_{int}				
R (a_0)	$E^{(2)}_{disp}$	$E^{(2)}_{ex\text{-}disp}$	ROHF +disp (TDDFT)	RCCSD(T)	RCCSD(T)/ DK	RCCSD(T)/ DK+b	CIPT2+Q/ DK	AQCC/ DK
4.50	−7287.1	2350.2	4311.4	5236.7	4878.1	4807.9	4742.4	5542.6
5.00	−5148.4	1373.4	646.2	1195.6	941.2	893.7	865.7	1503.9
5.25	−4339.8	1082.9	−126.0	273.4	67.6	26.1	11.0	574.6
5.50	−3663.5	867.4	−533.0	−254.1	−416.9	−454.3	−459.6	35.4
5.75				−534.4	−660.9	−695.1	−693.2	−260.0
6.00	−2619.5	573.1	−777.8	−663.6	−760.3	−791.9	−785.1	−406.7
6.25	−2217.9	469.2	−764.2	−703.2	−776.0	−805.7	−795.5	−465.2
6.50	−1879.1	384.7	−713.9	−692.0	−746.1	−774.0	−762.1	−473.7
6.75	−1593.0	315.3	−647.8	−654.1	−693.7	−719.8	−707.5	−455.3
7.00	−1351.2	258.2	−577.7	−603.8	−632.4	−656.4	−645.1	−424.2
7.50	−974.0	172.1	−448.4	−496.2	−510.1	−529.8	−522.4	−352.1
8.00	−704.3	113.6	−345.1	−399.8	−405.5	−421.2	−418.3	−286.1
9.00	−373.1	48.0	−209.0	−256.7	−255.3	−264.8	−267.9	−188.0
9.50	−273.8	30.9	−164.9	−205.4	−202.7	−210.1	−214.3	−152.2
10.00	−202.3	19.9	−130.9	−163.9	−160.8	−166.7	−171.0	−122.8
11.00	−112.9	8.2	−83.2	−103.8	−100.8	−104.8	−107.9	−79.1
12.00	−65.1	3.5	−53.2	−65.5	−63.1	−65.9	−67.7	−50.3

$$v^{pq}_{rs} \propto \sum_{l_X=1}^{\infty}\sum_{l_Y=1}^{\infty}\sum_{M=-l}^{l}(-1)^{l_X-l_Y+M}\begin{pmatrix} l_X & l_Y & l \\ m_X & m_Y & -M \end{pmatrix} \times \frac{\sqrt{2l+1}(Q^{m_X}_{l_X})^k_l (Q^{m_Y}_{l_Y})^m_n}{R^{l+1}}, \tag{6}$$

where $l=l_X+l_Y$ and $(Q^{m_Y}_{l_X})^k_l$ is the matrix element of the 2^{l_X}-pole moment operator of the monomer X (and analogously for the monomer Y). It should be noted that the above methodology can at present be applied only to the interacting S-state atoms.

III. *AB INITIO* RESULTS

A. Cr_2

We begin the discussion from the Cr_2 ($^{13}\Sigma^+_g$) interaction-for which there exist some experimental data.[11] This state is reasonably well represented using the single configuration as evidenced by the fact that the CASSCF and ROHF wave functions are practically the same. The DFT monomer calculations employed the B97-2 functional[44] with the Fermi-Amaldi asymptotic correction[45] which for the open-shell case involves two parameters one for the α-density and one for the β-density. These parameters were equal to 0.248 and 1.768 hartrees, respectively. The hybrid model combined V^{ROHF} with SAPT(DFT) dispersion and exchange-dispersion terms (ROHF+disp). The RCCSD(T) calculations were performed at three different levels of theory. The first included no scalar relativistic Douglas-Kroll-Hess[28,29] (DK) effects and employed the aug-cc-pVQZ (Ref. 46) basis set [denoted RCCSD(T)], so the direct comparison can be carried out with the SAPT(DFT) method for which the inclusion of relativistic effects is not yet implemented. Next, the RCCSD(T) calculations were performed with the inclusion of the Douglass-Kroll-Hess integrals and the aug-cc-pVQZ-DK (Ref. 46) basis set [denoted RCCSD(T)/DK]. The final RCCSD(T) calculation included this basis set augmented with a set of bond functions and DK relativistic correction [RCCSD(T)/DK+b]. The convergence of a CC iterative process in this high-spin system is difficult to achieve with basis sets involving diffuse orbitals because of intruder-state problems. The convergence problem was remedied using a level shift procedure (the shift value of 1 a.u. was sufficient for the CCSD convergence and the maximal value of T_1 diagnostic for all the runs was about 0.02). The CIPT2+Q and AQCC approaches employed a CASSCF reference function and both include the DK effects.

The results shown in Table I list the ROHF+disp values next to RCCSD(T) for a proper comparison. The ROHF +disp interaction energies agree reasonably well with the RCCSD(T) potential except for the discrepancies at short distances, where the RCCSD(T) is more repulsive and in the long range (see $R=12a_0$) where the ROHF+disp is less attractive. In the minimum region, the two potentials agree to within 10%. The similarity of the two potentials indicates that the binding of Cr_2 ($^{13}\Sigma^+_g$) originates from the dispersion interaction combined with its exchange counterpart. The exchange-dispersion energy represents a significant repulsive contribution, which quenches about 20% of the dispersion attraction in the minimum region. The scalar relativistic effects are fairly important for the quantitative description of this potential. The inclusion of the DK effects deepens the minimum of the RCCSD(T) potential by about 10%. The addition of bond functions, to optimize the dispersion interaction, further enhances the well depth by about 4%. This final potential is our most accurate result and the analytical fit is available upon request. The CIPT2+Q results are in very good agreement with the RCCSD(T) results. The AQCC treatment leads to a considerably underestimated potential at all distances.

The minimum characteristics, the long-range C_6 dispersion coefficient, and the dipole polarizability α, values are

TABLE II. Characteristics of the $^{13}\Sigma_g^+$ Cr_2 state.

Method	R_e (a_0)	$\bar{D}_e$ (cm^{-1})	C_6 (a.u.)	α (a.u.)
RCCSD(T)	6.30	704.1		
RCCSD(T)/DK	6.19	777.5	780[a]	82.9
RCCSD(T)/DK+b	6.18	807.8		
CIPT2+Q/DK	6.16	798.4	845	74.2
AQCC/DK	6.43	474.8	540	81.4
ROHF+disp(TDDFT)	6.06	779.1	626	75
Ref. 48			602.0	60.7
Ref. 11			733	
Ref. 50				78.3

[a]Obtained with frozen outer-core electrons (see the text).

shown in Table II. The three treatments, deemed reliable, lead to the well depths in the narrow range of values: 779.1 cm^{-1} (ROHF+disp), 798.4 cm^{-1} (CIPT2+Q/DK) and 807.8 cm^{-1} [RCCSD(T)/DK+b]. The position of the minimum occurs at a slightly shorter distance for the ROHF+disp potential ($R=6.06a_0$) compared to RCCSD(T)/DK+b ($R=6.18a_0$) and CIPT2+Q/DK ($R=6.16a_0$) due to the aforementioned underestimated short-range repulsion. The RCCSD(T)/DK+b potential was employed in the bound-state calculations using discrete variable representation.[47] The calculations predict the ground state of 776.8 cm^{-1}. Our final potential is notably deeper than the CASPT2 potential published by Pavlović *et al.*[14] which has the well depth of 576 cm^{-1}. The C_6 coefficients fitted to the long-range tail of the supermolecular potentials are 780, 645, and 540 a.u. for RCCSD(T)/DK, CIPT2+Q/DK, and AQCC/DK, respectively. It should be mentioned that the RCCSD(T) C_6 could only be fitted upon freezing the outer-core (3*s* and 3*p*) electrons. Otherwise a spurious lower-power R^{-1} term appeared at distances larger than $28a_0$. Our TDDFT C_6 coefficient calculated directly from Eq. (6) amounts to 626 a.u. This is in fairly good agreement with the result of Chu and Dalgarno[48] who employed time-dependent optimized effective potential with self-interaction correction. The experimental value of C_6 can be deduced from the measurements of Feshbach resonances in optically trapped ultracold Cr gas,[10] which are extremely sensitive to the long-range details of the Cr–Cr interaction potential. Two simulations of this experiment provide the values $C_6=733$ (with standard deviation of 70 a.u.)[11] and 770.[49] Our RCCSD(T) result is in very good agreement with these values, whereas the TDDFT result lies below the lower error bar. The higher TDDFT dispersion coefficients C_8 and C_{10} amount to 3.27×10^4 and 1.44×10^6, respectively. The available experimental result for the C_8 coefficient from the work of Werner *et al.*,[11] 7.5×10^4 a.u., is reportedly a weak upper bound for its value.

The calculations of static dipole polarizability of Cr, α, at various levels of theory offer additional clues concerning the performance of DFT and the role of correlation and relativistic effects on this property. Our DFT result for α is 75 a.u. which differs considerably from 60.7 a.u. obtained by Chu and Dalgarno[48] with a different variant of DFT.[48] The value recommended in their work amounts to 78 a.u. (see also Miller[50]) and both CIPT2 and AQCC results are in fairly good agreement. Our most accurate RCCSD(T)/DK treatment yields a slightly larger value of 82.9 a.u. The DK effects contribute about 5% toward lowering its value, consistent with previous findings for other first-row transition metals.[51] The core-valence correlation was found important in atomic properties, such as ionization energies and electron affinities of the 3*d* transition row.[52] To establish its effect on polarizabilities, we removed the outer-core electrons from the correlated space in the RCCSD(T) calculations. The result is a 10% increased α. Based on these observations, some calculations were also performed for Cr_2 with a larger core encompassing the 3*s* and 3*p* electrons. In the minimum region the RCCSD(T)/b calculations lead to a 5% deeper potential. We conclude that in the interaction potential of Cr_2 there is some degree of cancellation between the relativistic effects and the core-valence correlation.

B. Sc–Cr

The reference functions for $^8\Sigma^+$, $^8\Pi$, and $^8\Delta$ states of Sc–Cr were obtained from the state-averaged CASSCF calculations. In the C_{2v} group the Σ^+, Π, and Δ representations correlate with A_1, B_1+B_2, and A_1+A_2, respectively. The state symmetries were distinguished by the calculated values of Λ. The CASSCF calculations employed a valence active space in which the 4*s* orbital of Sc was initially kept doubly occupied. The latter was necessary to prevent root flipping which made the projection on the specific value of Λ impossible. The CASSCF wave functions were used in the MRCI calculations. Proper starting vectors for the ROHF calculations for the three states were obtained by canonicalization of the CASSCF natural orbitals. The ROHF vectors were subsequently used in RCCSD(T) calculations and as the zeroth-order functions in the SAPT method. The RCCSD(T) calculations were performed with averaged atomic natural orbital (ANO) basis sets of Bauschlicher[53] and Partridge[54] with two types of core. The results below were obtained with the *KL* electrons kept in core [denoted RCCSD(T)]. The RCCSD(T) calculations which included the DK effects are denoted RCCSD(T)/DK. The calculations employed a level shift and the T_1 diagnostics did not exceed 0.02. No DK effects were considered in the MRCI calculations. The SAPT treatment employed the TDHF polarization propagator to evaluate state-dependent dispersion and exchange-dispersion energies. In the hybrid model, these terms are combined with CASSCF interaction energy to at least partially account for nondynamic correlation effects (denoted CAS+disp).

The adiabatic potentials for the three octet states of Sc–Cr are displayed in Fig. 1 and the minimum characteristics are listed in Table III. At the CASSCF level of theory [Fig. 1(a)], all the three states are repulsive with the Σ^+ state being considerably more repulsive than Π and Δ. The analogous curves evaluated at the ROHF level of theory are slightly less repulsive, but generally very close to those from CASSCF. At $R=6a_0$ the differences are 63 cm^{-1} for Σ^+, 10 cm^{-1} for Π, and 33 cm^{-1} for Δ. The RCCSD(T) adiabatic curves [Fig. 1(b)] have deep minima (Δ: 3958 cm^{-1}, Π: 3531 cm^{-1}, and Σ^+: 2871 cm^{-1}) occurring at the narrow range of $R=5.7a_0-5.8a_0$. Freezing the outer-core electrons has a small effect (less than 2%) on the well depths, whereas

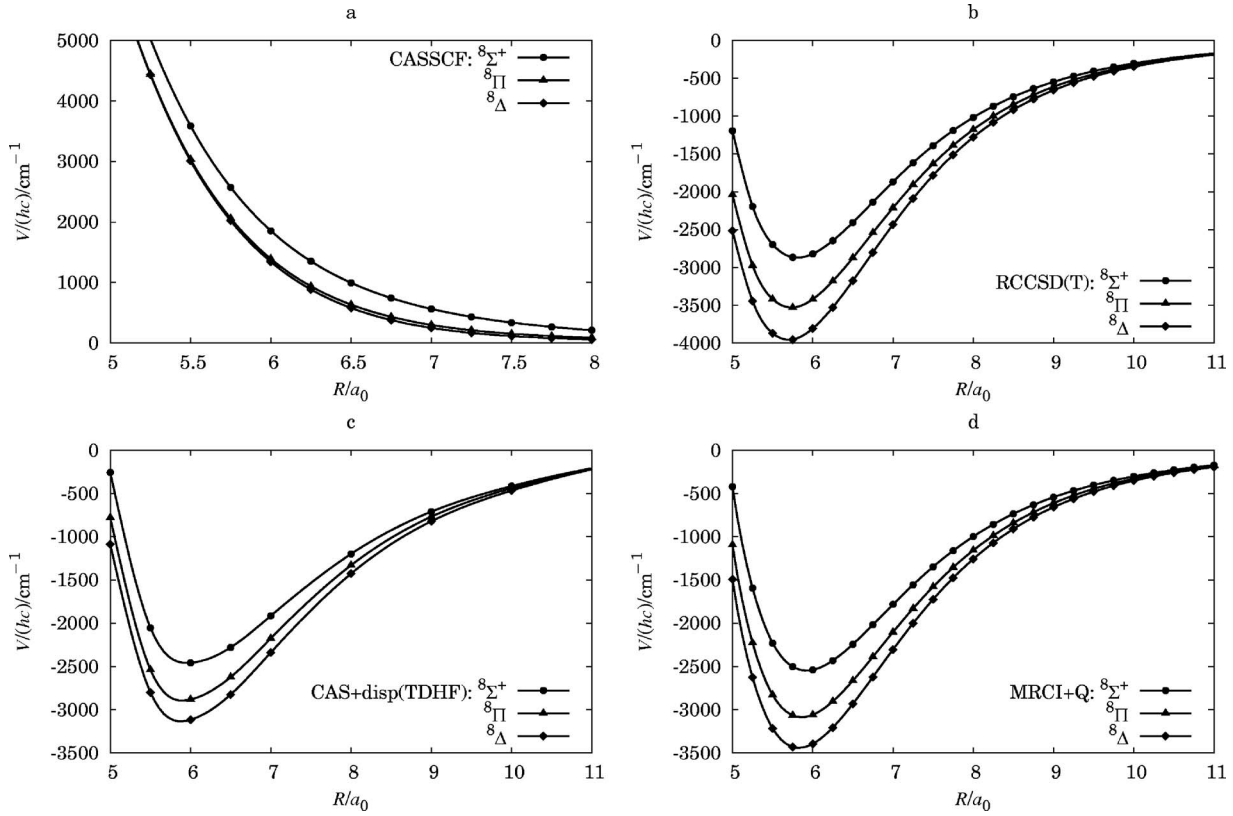

FIG. 1. Interaction potentials for $^8\Sigma^+$, $^8\Pi$, and $^8\Delta$ states of Sc–Cr obtained at the following levels of theory: (a) CASSCF, (b) RCCSD(T), (c) CAS+disp(TDHF), (d) MRCI+Q.

the inclusion of the DK effects leads to further stabilization of about 240–250 cm^{-1} and shortening of R_e by about $0.1a_0$. The hybrid model CAS+disp results in the three potentials which are in qualitative agreement with RCCSD(T), although uniformly shallower [Fig. 1(c)]. Their minima occur at slightly longer distances $R=5.92a_0$. Finally, the relative order of the three states is confirmed by the MRCI results [Fig. 1(d)]. The binding in these states clearly originates from correlation effects, the origins of which are quite interesting. To examine their nature we compare the correlation part of the interaction energy obtained at the RCCSD(T) level of theory, V^{corr}, with the sum of the dispersion and exchange-dispersion terms for the three states. The result for the most attractive state Δ (where the agreement is the least favorable) is shown in Fig. 2. The figure also displays the dispersion energy alone. The agreement between these quantities is excellent and the discrepancies, which occur at short and long distances, respectively, are not unexpected. Specifically, in the short range the present formulation of exchange dispersion (and the S^2 approximation) is expected to deterio-

TABLE III. Minimum characteristics and the dispersion coefficients of the Sc–Cr system.

State	Method	R_e (a_0)	$\bar{D}_e$ (cm^{-1})	$C_{6,0}$ (a.u.)	$C_{6,2}$ (a.u.)
$^8\Sigma^+$	RCCSD(T)	5.81	2871		
	RCCSD(T)/DK	5.71	3118		
	MRCI+Q	5.92	2548		
	CAS+disp(TDHF)	6.01	2459		
$^8\Pi$	RCCSD(T)	5.73	3531		
	RCCSD(T)/DK	5.65	3767		
	MRCI+Q	5.86	3087		
	CAS+disp(TDHF)	5.95	2886		
$^8\Delta$	RCCSD(T)	5.70	3958		
	RCCSD(T)/DK	5.62	4209		
	MRCI+Q	5.83	3442		
	CAS+disp(TDHF)	5.92	3124		
V_0	SAPT			1366	
V_2	SAPT				−48.7

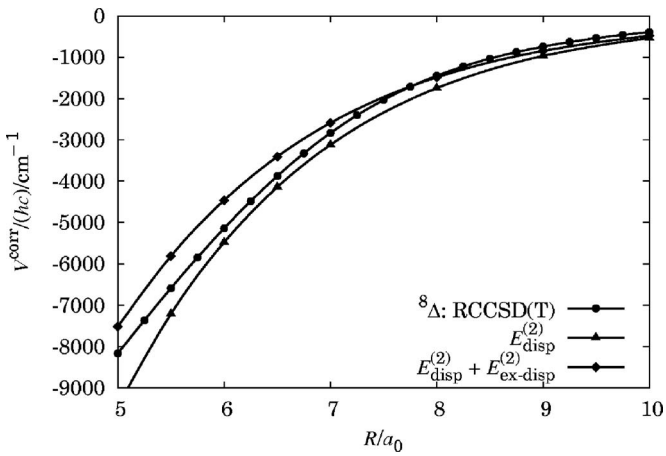

FIG. 2. Comparison of the correlation contribution to the RCCSD(T) interaction energies, V^{corr}, with dispersion and exchange-dispersion energies for $^8\Delta$ state of the Sc–Cr system.

rate. In the long range, where the exchange effects are no longer important, the TDHF and CCSD(T) descriptions of the dispersion energy may show discrepancies (although there are known open-shell cases where the two treatments agree very well; see Ref. 25). One remarkable feature is the sheer magnitude of dispersion energy, which is not seen in van der Waals interactions of main-group elements except for alkali metal and alkaline earth atom dimers. However, in the latter cases it is matched with a very large exchange counterpart.[55,56] It is interesting to examine factors contributing to considerable splittings between potentials. Let us consider the difference between the Σ^+ and Π states at $R=6a_0$ which in CAS+disp amounts to 423 cm^{-1}. CASSCF contributes the largest share to this difference, 465 cm^{-1}. The contribution from the dispersion is −61 cm^{-1}, and the one from the exchange dispersion is 19 cm^{-1}. By comparison, the analogous energy difference in RCCSD(T) is 600 cm^{-1}.

Another interesting aspect is the strengthening of the interaction compared to Cr_2. Substituting Sc for Cr results in a 3.6 (Σ^+)-, 4.3 (Π)-, and 4.9 (Δ)-fold increase in stabilization compared with Cr–Cr. To explain this effect, three factors in order of increasing importance can be identified. First, the V^{CASSCF} curves for the Δ and Π states of Sc–Cr are considerably less repulsive (and slightly less repulsive for Σ^+) than those of Cr_2 for $R>6a_0$. Second, the average C_6 coefficient of the Sc–Sc interaction is 2.3 times larger than that of Cr–Cr.[48] The third is the considerable 50% decrease in the highest occupied molecular orbital–lowest unoccupied molecular orbital gap between Sc–Cr and Cr_2. The latter may be responsible for the violation of combination rules.[57] Our TDHF value of $C_{6,0}=1366$ a.u. for Sc–Cr, which is very close to the Sc–Sc value $C_6=1383$ a.u. of Chu and Dalgarno,[48] seems to indicate such a violation.

Our lowest state, $^8\Delta$, can be compared with the DFT result of Gutsev *et al.*[12] who identified the lowest octet state as $^8\Pi$. Although their assignment is approximate because of unrestricted KS formalism, the other characteristics of this state are in reasonable agreement with our RCCSD(T) findings. The position of the minimum agrees quite well (our value $5.62a_0$ versus $5.51a_0$) and so does the small value of the dipole moment. Unfortunately, they do not report the well-depth value. One interesting insight from the work of Gutsev *et al.*[12] concerns the type of bonding in this state. Their analysis indicates that it involves a single bond between the 4*s* orbitals of Sc and Cr. This may provide an additional explanation for our observed strength of this state.

C. Sc–Kr

By substituting semiclosed Cr atom in Sc–Cr by closed-shell Kr, we can better understand the above results for Sc–Cr by comparing and contrasting it with a typical van der Waals complex Sc–Kr. Such calculations will also allow us to further demonstrate interpretative capabilities of SAPT.

The ROHF wave functions for the $^2\Sigma^+$, $^2\Pi$, and $^2\Delta$ states of Sc–Kr were obtained by the single occupation of Sc $3d_\sigma$, $3d_\pi$, or $3d_\delta$ orbitals, respectively. These functions were used as the starting point for the RCCSD(T) calculations and as the zeroth-order wave functions in SAPT. The SAPT method employed TDHF polarization propagator in the calculation of the dispersion energy. This term, along with its exchange counterpart, was combined with V^{ROHF} to yield the hybrid SAPT model, ROHF+disp(TDHF). The ANO basis set[53,54] was used for Sc and the aug-cc-pVQZ basis set[58] for Kr.

TABLE IV. Minimum characteristics and the dispersion coefficients of the Sc–Kr system.

State	Method	R_e (a_0)	$\bar{D}_e$ (cm^{-1})	$C_{6,0}$ (a.u.)	$C_{6,2}$ (a.u.)
$^2\Sigma^+$	RCCSD(T)	9.536	84.0		
	ROHF+disp(TDHF)	9.37	93.7		
$^8\Pi$	RCCSD(T)	9.463	85.8		
	ROHF+disp(TDHF)	9.35	93.2		
$^2\Delta$	RCCSD(T)	9.646	81.2		
	ROHF+disp(TDHF)	9.52	89.0		
V_0	RCCSD(T)			350	
V_0	SAPT			382	
V_2	RCCSD(T)				−0.62
V_2	SAPT				−5.9

The results for the $^2\Sigma^+$, $^2\Pi$, and $^2\Delta$ states are reported in Table IV and in Figs. 3 and 4. As seen in Table IV the complex is very weakly bound with the well depths of 81–86 cm^{-1} [RCCSD(T)] or 89–94 cm^{-1} (ROHF+disp). The minima of the three potentials occur at large distances, around $9.4a_0-9.6a_0$. The ROHF+disp model agrees very well with RCCSD(T) in describing these characteristics. Both approaches predict the Δ state to be the least stable and Σ^+ and Π to be very close. The minimum region in Sc–Kr is pushed toward longer distances than in Sc–Cr because of much stronger exchange repulsion in the former as evidenced by a comparison of the ROHF potential curves for Sc–Kr in Fig. 3 with the three CASSCF potentials of Sc–Cr in Fig. 1(a). For example, the three sets of curves if compared at the same distance, for example, $R=6.5a_0$, reveal approximately 2.5 larger repulsion in Sc–Kr than in Sc–Cr. The $^2\Sigma^+$ state of Sc–Kr is the most repulsive at short distances just as in Sc–Cr; however, at around $6.8a_0$ a crossing

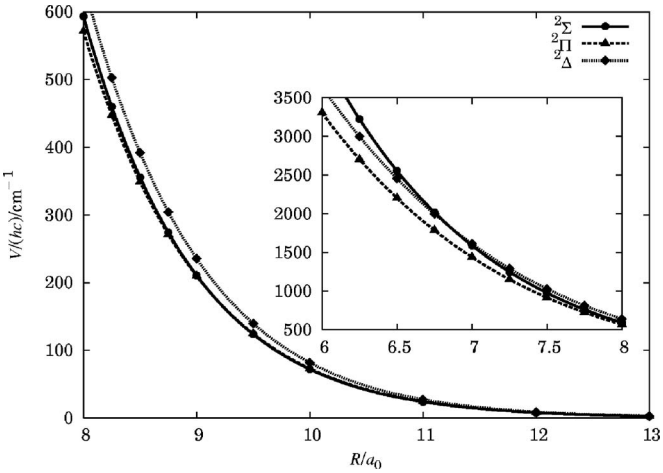

FIG. 3. ROHF interaction energies for the Sc–Kr system (minimum at approximately $9.5a_0$). The outer figure shows the region of minimum, while the inset shows a short range.

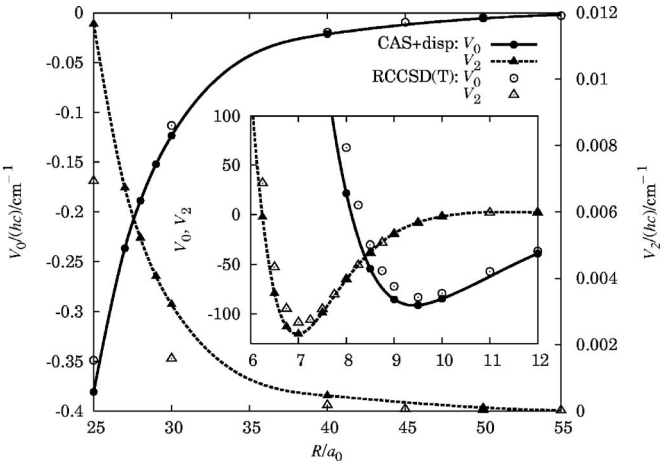

FIG. 4. ROHF+disp and RCCSD(T) isotropic (V_0) and anisotropic (V_2) components of interaction potential for the Sc–Kr system. The outer figure shows the asymptotic region, while the inset shows the minimum region.

occurs and the $^2\Delta$ state becomes the most repulsive. This ordering of the ROHF curves $^2\Delta > ^2\Pi \approx ^2\Sigma^+$ at distances of $9.5a_0$ determines the order of minima in the full interaction potentials.

The isotropic V_0 and anisotropic V_2 parts [see Eq. (4)] of the full RCCSD(T) and ROHF+disp potentials are shown in Fig. 4. The ROHF+disp and RCCSD(T) values agree reasonably well in the minimum regions of V_0 and V_2. In the asymptotic region, a similar agreement is seen in V_0 but there are some discrepancies in V_2. Consequently, the dispersion coefficients $C_{6,0}$ (see Table IV) obtained by both methods are very similar, while $C_{6,2}$ differ quantitatively (although both methods predict them to be small). The average $C_{6,0}$ dispersion coefficient of Sc–Kr is 3.6 times smaller than that of Sc–Cr (see Table III), which is consistent with the ratio of dipole polarizabilities of Cr and Kr (4.6). The dispersion coefficients $C_{6,2}$ (see Table IV) of both systems are both negative but differ by one order of magnitude. According to Eq. (4), the negative sign of $C_{6,2}$ indicates that Δ is the lowest state in the asymptotic region. Thus, the order of states in Sc–Kr is different in the minimum and in the asymptotic region. As mentioned above the order in the minimum region is due to the exchange repulsion, whereas that in the long-range results from the dispersion interaction. The source of the long-range anisotropy of dispersion energy in both complexes is the single $3d$ electron of Sc which also gives rise to polarizability anisotropy. It is difficult to rationalize at this point why RCCSD(T) and SAPT lead to significantly different values of $C_{6,2}$. More work along these lines is necessary.

D. Spin-orbit coupling

In the doublet-state Sc–Kr complex the Sc atom is the source of both the orbital **L** and spin **S** angular momenta. This is not the case for the octet state of Sc–Cr which in itself arises from the coupling of the spin momenta of both atoms. The following discussion applies primarily to Sc–Kr but also offers some hints for a treatment of Sc–Cr. The total electronic angular momentum of a spin-orbit coupled state is denoted $\mathbf{J}=\mathbf{L}+\mathbf{S}$ and the basis set is $|J,M_J\rangle$. In this basis set the spin-orbit Hamiltonian $\hat{H}_{\mathrm{SO}}=a\mathbf{L}\cdot\mathbf{S}$ is diagonal. The spin-orbit parameter a for Sc is 67.336 cm^{-1}.[59] Assuming that a is constant with R, the Sc–Kr interaction represents a limiting case where the splitting between the adiabatic potentials is small compared to a. The matrix of $\hat{V}+\hat{H}_{\mathrm{SO}}$ in this basis set is block diagonal with the following diagonal elements:

$$\begin{aligned}
\left\langle \tfrac{5}{2},\pm\tfrac{5}{2}\middle|\hat{V}\middle|\tfrac{5}{2},\pm\tfrac{5}{2}\right\rangle &= V_\Delta + a,\\
\left\langle \tfrac{5}{2},\pm\tfrac{3}{2}\middle|\hat{V}\middle|\tfrac{5}{2},\pm\tfrac{3}{2}\right\rangle &= \tfrac{1}{5}(4V_\Pi + V_\Delta) + a,\\
\left\langle \tfrac{5}{2},\pm\tfrac{1}{2}\middle|\hat{V}\middle|\tfrac{5}{2},\pm\tfrac{1}{2}\right\rangle &= \tfrac{1}{5}(3V_\Sigma + 2V_\Pi) + a,\\
\left\langle \tfrac{3}{2},\pm\tfrac{3}{2}\middle|\hat{V}\middle|\tfrac{3}{2},\pm\tfrac{3}{2}\right\rangle &= \tfrac{1}{5}(V_\Pi + 4V_\Delta) - \tfrac{3}{2}a,\\
\left\langle \tfrac{3}{2},\pm\tfrac{1}{2}\middle|\hat{V}\middle|\tfrac{3}{2},\pm\tfrac{1}{2}\right\rangle &= \tfrac{1}{5}(2V_\Sigma + 3V_\Pi) - \tfrac{3}{2}a,
\end{aligned} \tag{7}$$

and the following nonzero off-diagonal elements:

$$\begin{aligned}
\left\langle \tfrac{5}{2},-\tfrac{3}{2}\middle|\hat{V}\middle|\tfrac{3}{2},-\tfrac{3}{2}\right\rangle &= \tfrac{2}{5}(V_\Pi - V_\Delta),\\
\left\langle \tfrac{5}{2},-\tfrac{1}{2}\middle|\hat{V}\middle|\tfrac{3}{2},-\tfrac{1}{2}\right\rangle &= \tfrac{\sqrt{6}}{5}(V_\Sigma - V_\Pi),\\
\left\langle \tfrac{5}{2},\tfrac{1}{2}\middle|\hat{V}\middle|\tfrac{3}{2},\tfrac{1}{2}\right\rangle &= \tfrac{\sqrt{6}}{5}(V_\Pi - V_\Sigma),\\
\left\langle \tfrac{3}{2},\tfrac{3}{2}\middle|\hat{V}\middle|\tfrac{5}{2},\tfrac{3}{2}\right\rangle &= \tfrac{2}{5}(V_\Delta - V_\Pi).
\end{aligned} \tag{8}$$

The SO adiabats are obtained as the eigenvalues of the above matrix substituting the RCCSD(T) V_Σ, V_Π, and V_Δ potentials. They are subsequently shifted to their respective asymptotes, $J=\frac{5}{2}$ and $J=\frac{3}{2}$, for comparison purposes. The minimum positions in the SO adiabats remain virtually unchanged from their spin-free positions. The interaction energies compared at $R=9.5a_0$ (i.e., in the minimum region) vary between -85.03 cm^{-1} ($|\frac{3}{2},\frac{1}{2}\rangle$) and -80.62 cm^{-1} ($|\frac{5}{2},\frac{5}{2}\rangle = V_\Delta$). The energy of the lowest $|\frac{3}{2},\frac{1}{2}\rangle$ state is very close to that of the lowest spin-free adiabat V_Π (see Table IV). We conclude that this complex should not be affected by the SO coupling as long as the a parameter remains constant with R. The octet Sc–Cr complex presents an opposite case, where the splitting between the adiabatic potentials is one order of magnitude larger than a. However, its treatment is much more complicated (if not intractable) because $\hat{H}_{\mathrm{SO}}$ is expected to couple also the states of lower multiplicity about which nothing is known at this point. If, in the first approximation, one assumes these couplings to be negligible, the ground state Δ will be unaffected by the SO coupling.

IV. SUMMARY AND CONCLUSIONS

We have presented results for two transition metal dimers in their high-spin van der Waals states, ($^{13}\Sigma_g^+$) Cr_2 and ($^8\Sigma^+, ^8\Pi, ^8\Delta$) Sc–Cr. To aid the analysis of these interactions, a typical van der Waals complex Sc–Kr involving the $^2\Sigma^+$, $^2\Pi$, $^2\Delta$ manifold has also been studied. The interaction potentials have been calculated by a supermolecular method based on the single-reference RCCSD(T) and on a number of multireference approaches including CIPT2, MRCI, and

AQCC. In addition, we report the open-shell SAPT TDHF dispersion and exchange-dispersion energies for the manifolds of the three states in Sc–Cr and Sc–Kr. In the case of Cr_2 the open-shell SAPT(DFT) was applied in the calculations of the dispersion and exchange-dispersion terms with the TDDFT polarization propagator. The present TM systems pose a very demanding environment for testing these theories. Dispersion and exchange-dispersion energies combined with the supermolecular (purely repulsive) ROHF or CASSCF interaction potentials (CAS+disp, ROHF+disp models, respectively) provide reasonable qualitative results and with substantially less effort than that required to judiciously apply the supermolecular treatments used here. SAPT also proves useful in calculations of properties depending on asymptotic parts of the interaction potentials, such as dispersion coefficients.

The $^{13}\Sigma_g^+$ state of Cr_2 is bound by a midrange van der Waals interaction with the well depth of about 800 cm^{-1}. RCCSD(T), CIPT2, and ROHF+disp are in reasonable agreement with each other. The predictions of the C_6 dispersion coefficient are in reasonable agreement with experiment and previous calculations. Our well depth, however, is much deeper than that of the previously reported CASPT2 potential.[14] SAPT(DFT) reveals a significant role of exchange dispersion in open-shell interactions. This term is seen to more strongly quench the dispersion than in the closed-shell systems of comparable strength.

In Sc–Cr the CASSCF potentials are purely repulsive for the three states and the post-CASSCF correlation effects lead to a relatively strong bonding in all three states. The ordering of well depths from the RCCSD(T) calculations is $^8\Delta$ (about 4000 cm^{-1}), $^8\Pi$ (about 3600 cm^{-1}), and $^8\Sigma^+$ (about 2900 cm^{-1}). Three approaches applied to this system, RCCSD(T), MRCI, and CAS+disp, confirm this ordering although the values differ. The splitting of adiabatic potentials is considerable (400–600 cm^{-1}) and dominated by the differences in the CASSCF repulsion. In view of the strong anisotropy of interactions, the prospects for the sympathetic cooling of a Sc–Cr mixture are unlikely because the relaxation processes will be very fast. It is also expected that the spin-orbit effects will be of secondary importance. The source of the bonding is a very strong dispersion energy.

Sc–Kr is a typical van der Waals complex bound by less than 100 cm^{-1} and with very small splittings among the states. The order of well depths is $^2\Pi \approx {}^2\Sigma^+ > {}^2\Delta$ at the RCCSD(T) and ROHF+disp levels of theory. Both approaches lead to a good agreement for V_0 and V_2.

ACKNOWLEDGMENTS

The authors thank Alexei Buchachenko, Piotr Piecuch, and Bogumił Jeziorski for helpful advice in various aspects of this study. This work was supported by the National Science Foundation under Grant No. CHE-0414241. P.S.Z. wishes to acknowledge the support of the Foundation for the Polish Science. J.K. was supported by NSF grant (CHE-0413743) to Millard H Alexander.

[1] G. Frenking and N. Frohlich, Chem. Rev. (Washington, D.C.) **100**, 717 (2000).
[2] J. F. Harrison, Chem. Rev. (Washington, D.C.) **100**, 679 (2000).
[3] S. R. Langhoff and C. W. Bauschlicher, Annu. Rev. Phys. Chem. **39**, 181 (1988); C. W. Bauschlicher, H. Partridge, S. R. Langhoff, and M. Rosi, J. Chem. Phys. **95**, 1057 (1991).
[4] M. D. Morse, Chem. Rev. (Washington, D.C.) **86**, 1049 (1986).
[5] C. I. Hancox, S. Doret, M. Hummon, R. Krems, and J. Doyle, Phys. Rev. Lett. **94**, 013201 (2005).
[6] J. Kłos, M. F. Rode, J. E. Rode, G. Chałasiński, and M. M. Szcześniak, Eur. Phys. J. D **31**, 429 (2004).
[7] J. Stuhler, A. Griesmaier, T. Koch, M. Fattori, T. Pfau, S. Giovanazzi, P. Pedri, and L. Santos, Phys. Lett. A **95**, 150406 (2005).
[8] R. Krems, J. Kłos, M. Rode, M. M. Szcześniak, G. Chałasiński, and A. Dalgarno, Phys. Rev. Lett. **94**, 013202 (2005).
[9] J. D. Weinstein, R. deCarvalho, J. Kim, D. Patterson, B. Friedrich, and J. M. Doyle, Phys. Rev. A **57**, R3173 (1998).
[10] A. Griesmaier, J. Werner, S. Hensler, J. Stuhler, and T. Pfau, Phys. Rev. Lett. **94**, 160401 (2005).
[11] J. Werner, A. Griesmeier, S. Hensler, J. Stuhler, T. Pfau, A. Simoni, and E. Tiesinga, Phys. Rev. Lett. **94**, 183201 (2005).
[12] G. L. Gutsev, P. Jena, B. K. Rao, and S. N. Khanna, J. Chem. Phys. **114**, 10738 (2001).
[13] G. L. Gutsev, M. D. Mochena, P. Jena, C. W. Bauschlicher, Jr., and H. Partridge, III, J. Chem. Phys. **121**, 6785 (2004).
[14] Z. Pavlović, B. O. Roos, R. Côté, and H. R. Sadeghpour, Phys. Rev. A **69**, 030701 (2004).
[15] S. V. Nguyen, J. S. Helton, K. Maussang, W. Ketterle, and J. M. Doyle, Phys. Rev. A **71**, 025602 (2005).
[16] P. Celani, H. Stoll, H.-J. Werner, and P. J. Knowles, Mol. Phys. **102**, 2369 (2004).
[17] P. S. Żuchowski, R. Podeszwa, R. Moszyński, K. Szalewicz, and B. Jeziorski (unpublished).
[18] P. J. Knowles, C. Hampel, and H.-J. Werner, J. Chem. Phys. **99**, 5219 (1993).
[19] M. Gutowski, F. B. van Duijneveldt, G. Chałasiński and L. Piela, Mol. Phys. **61**, 233 (1987); J. A. Kłos, M. M. Szcześniak and G. Chałasiński, Int. Rev. Phys. Chem. **23**, 541 (2004).
[20] G. Chałasiński and K. Szalewicz, Int. J. Quantum Chem. **18**, 1071 (1980).
[21] S. M. Cybulski, R. Burcl, G. Chałasiński, and M. M. Szcześniak, J. Chem. Phys. **103**, 10116 (1995).
[22] S. M. Cybulski, G. Chałasiński, and M. M. Szcześniak, J. Chem. Phys. **105**, 9525 (1996).
[23] S. M. Cybulski, R. Burcl, M. M. Szcześniak, and G. Chałasiński, J. Chem. Phys. **104**, 7997 (1996).
[24] J. Kłos, G. Chałasiński, M. T. Berry, R. Bukowski, and S. M. Cybulski, J. Chem. Phys. **112**, 2195 (2000).
[25] P. S. Żuchowski, B. Bussery-Honvault, R. Moszyński, and B. Jeziorski, J. Chem. Phys. **119**, 10497 (2003).
[26] H. Hettema and P. E. S. Wormer, J. Chem. Phys. **93**, 3389 (1990).
[27] S. Atahan, J. Kłos, P. S. Żuchowski, and M. H. Alexander, Phys. Chem. Chem. Phys. **8**, 4420 (2006).
[28] M. Douglas and N. M. Kroll, Ann. Phys. (N.Y.) **82**, 89 (1974).
[29] G. Jansen and B. A. Hess, Phys. Rev. A **39**, 6016 (1989).
[30] P. G. Szalay and R. J. Bartlett, J. Chem. Phys. **103**, 3600 (1995).
[31] H.-J. Werner and P. J. Knowles, J. Chem. Phys. **89**, 5803 (1988).
[32] P. J. Knowles and H.-J. Werner, Chem. Phys. Lett. **145**, 514 (1988).
[33] R. Moszyński, B. Jeziorski, and K. Szalewicz, Int. J. Quantum Chem. **45**, 409 (1993).
[34] R. McWeeny, Croat. Chem. Acta **57**, 865 (1984).
[35] M. Jaszuński and R. McWeeny, Mol. Phys. **55**, 1275 (1985).
[36] S. F. Boys and F. Bernardi, Mol. Phys. **19**, 553 (1970).
[37] J. A. Kłos, G. Chałasiński, M. M. Szcześniak, and H.-J. Werner, J. Chem. Phys. **115**, 3085 (2001).
[38] R. Ahlrichs, R. Penco, and G. Scoles, J. Chem. Phys. **19**, 119 (1977).
[39] C. F. Kuntz, C. Hattig, and B. A. Hess, Mol. Phys. **89**, 139 (1996).
[40] H.-J. Werner, P. J. Knowles, R. Lindh, F. R. Manby, M. Schütz, P. Celani, T. Korona, G. Rauhut, R. D. Amos, A. Bernhardsson *et al.*, MOLPRO, version 2006.1, a package of *ab initio* programs (2006), see http://www.molpro.net
[41] R. Bukowski, W. Cencek, P. Jankowski, B. Jeziorski, M. Jeziorska, S. A. Kucharski, V. F. Lotrich, A. J. Misquitta, R. Moszyński, K. Patkowski *et al.*, SAPT2006, an *ab initio* program for many-body symmetry-adapted perturbation theory calculations of intermolecular interaction energies (2006), see http://www.physics.udel.edu/~szalewic/SAPT/SAPT.html

[42] V. Aquilanti and G. Grossi, J. Chem. Phys. **73**, 1165 (1980).
[43] R. Krems and A. Dalgarno, *Fundamental World of Quantum Chemistry* (Kluwer, Dordrecht, 2004), Vol. 3, pp. 273–294.
[44] P. J. Wilson, T. J. Bradley, and D. J. Tozer, J. Chem. Phys. **115**, 9233 (2001).
[45] D. J. Tozer and N. C. Handy, J. Chem. Phys. **109**, 10180 (1998).
[46] N. B. Balabanov and K. Peterson, J. Chem. Phys. **123**, 064107 (2005).
[47] D. T. Colbert and W. H. Miller, J. Chem. Phys. **96**, 1982 (1992).
[48] X. Chu and A. Dalgarno, J. Chem. Phys. **121**, 4083 (2004).
[49] Z. Pavlović, R. V. Krems, R. Côté, and H. R. Sadeghpour, Phys. Rev. A **71**, 061402 (2005).
[50] T. M. Miller, *CRC Handbook of Chemistry and Physics*, 79th ed. (CRC, Boca Raton, FL, 1998), pp. 160–174.
[51] J. A. Kłos, J. Chem. Phys. **123**, 024308 (2005).
[52] N. B. Balabanov and K. Peterson, J. Chem. Phys. **125**, 074110 (2006).
[53] C. W. Bauschlicher, Jr., Theor. Chim. Acta **92**, 183 (1995).
[54] H. Partridge, J. Chem. Phys. **90**, 1043 (1989).
[55] W. T. Zemke and W. C. Stwalley, J. Chem. Phys. **111**, 4956 (1999).
[56] B. Bussery-Honvault, J.-M. Launay, and R. Moszyński, Phys. Rev. A **68**, 032718 (2003).
[57] G. Maitland, M. Rigby, B. Smith, and W. Wakeham, *Intermolecular Forces: Their Origin and Determination* (Clarendon, Oxford, 1987).
[58] D. E. Woon and T. H. Dunning, Jr., J. Chem. Phys. **98**, 1358 (1993).
[59] *NIST handbook of basic atomic spectroscopic data*, see http://www.physics.nist.gov/PhysRefData/Handbook.